JOURNAL OF SOLID STATE CHEMISTRY **140,** 62–70 (1998)
ARTICLE NO. SC987854

Thermal Behavior of Zinc Phenylphosphonate and Structure Determination of γ-$Zn_2P_2O_7$ from X-Ray Powder Diffraction Data

T. Bataille, P. Bénard-Rocherullé, and D. Louër

Laboratoire de Chimie du Solide et Inorganique Moléculaire (UMR CNRS 6511), Groupe de Cristallochimie, Université de Rennes I, Avenue du Général Leclerc, 35042 Rennes Cedex, France

Received December 15, 1997; in revised form April 14, 1998; accepted April 23, 1998

The thermal behavior of zinc phenylphosphonate has been studied by temperature-dependent X-ray powder diffraction and thermo-gravimetry in the temperature range 19–600°C. The different phases occurring during the decomposition have been identified, i.e., the anhydrous phase and the three successive polymorphic varieties of $Zn_2P_2O_7$. The first one is amorphous, δ-$Zn_2P_2O_7$ is poorly crystalline, and γ-$Zn_2P_2O_7$ is a metastable phase. The last transforms into the β variety at higher temperature. The crystal structure of γ-$Zn_2P_2O_7$ has been solved *ab initio* from powder diffraction data collected with conventional monochromatic X-rays. The symmetry is orthorhombic with the cell dimensions a = 4.9504(5) Å, b = 13.335(2) Å, c = 16.482(3) Å, space group *Pbcm*, Z = 8. The structure consists of infinite corrugated chains of ZnO_5 trigonal bipyramids, running along [001]. These chains are linked together by P_2O_7 groups in the two other directions. The $P_2O_7^{4-}$ anions display low angles and an eclipsed conformation, contrary to the α and β phases.

INTRODUCTION

In recent years the synthesis and crystal chemistry of various layered metal phosphonates have received considerable attention, including zinc compounds (1–11). However, only a few studies have described their thermal behavior. Some elements of the thermal decomposition of zinc phenylphosphonate monohydrate were reported by Frink *et al.* (6), showing the formation of the anhydrous phase, but the next stages of the decomposition were not completely elucidated. On the other hand, in a recent work on uranium phenylphosphonate it has been shown that uranyl diphosphate is formed from thermal decomposition (12). Also, zinc diphosphates have been observed among the decomposition products of related zinc di(*tert*-butyl)phosphate complexes (13). It is then of interest to reconsider thoroughly the different stages of the decomposition of zinc phenylphosphonate, both to elucidate the decomposition mechanism and to know if zinc diphosphate is formed as final product. There is here an additional interest in the study since several polymorphs of $Zn_2P_2O_7$ have been reported in literature (14). Among them, the crystal structures of the α and β phases, determined from single-crystal studies, have been described (15, 16). For two other varieties, unindexed powder diffraction data for γ-$Zn_2P_2O_7$ (17) and for another metastable modification (18) were reported.

The study of the thermal behavior of solids has greatly benefited in the recent years from the development of temperature-dependent X-ray powder diffraction with conventional X-ray sources (19). It is of interest to extend the field of applications to different classes of solids, such as precursors of new oxide materials. This technique is applied here to investigate the behavior of $Zn(O_3PC_6H_5)\cdot H_2O$ in order to identify the phases occurring during the thermal decomposition. As expected, it is demonstrated that zinc diphosphates are formed in the final stages, particularly the metastable phase γ-$Zn_2P_2O_7$. Consequently, the present study deals with the thermal decomposition of zinc phenylphosphonate, the description of the stability conditions of zinc diphosphate polymorphs, and the *ab initio* crystal structure determination of γ-$Zn_2P_2O_7$, from powder diffraction data collected with conventional monochromatic X-rays.

EXPERIMENTAL

Material Preparation

Zinc phenylphosphonate, $Zn(O_3PC_6H_5)\cdot H_2O$, was synthesized according to methods reported in literature (see Ref. (6)), though zinc nitrate was used instead of zinc chloride. 0.1 M solutions of phenylphosphonic acid and zinc nitrate were mixed in equimolar ratios, and the pH was adjusted to 6. The resulting mixture was refluxed and kept at 70°C for 1 day. The white precipitate obtained was filtered off, washed with distilled water and ethanol (95%), and, finally, dried at 40°C. The compound formed was characterized by X-ray diffraction and identified as pure zinc phenylphosphonate monohydrate (3).

Density measurements of the decomposition products were carried out with an automatic helium picnometer AccuPyc 1330 (Micromeritics).

0022-4596/98 $25.00

Thermal Analyses

Temperature-dependent X-ray diffraction (TDXD) was performed with a powder diffractometer combining the curved position-sensitive detector from INEL (CPS 120) and a high temperature attachment from Rigaku. The detector was used in a semi-focusing arrangement by reflection (Cu$K\alpha_1$ radiation, $\lambda = 1.5406$ Å) as described elsewhere (20). With this geometry the flat sample is stationary. An 4° angle between the incident beam and the surface of the sample was selected. The thermal decomposition of $Zn(O_3PC_6H_5)\cdot H_2O$ was carried out in flowing air with heating rates of 25°C h^{-1} until 300°C and 15°C h^{-1} to 600°C. To ensure satisfactory counting statistics, a counting time of 2000 s per pattern was selected.

TG analyses were carried out with a Rigaku Thermoflex instrument. The 20 mg powdered samples were spread evenly in a large sample holder to avoid mass effects. The TG runs were performed in flowing air with a heating rate of 10°C h^{-1} from room temperature to 900°C.

High-Resolution Powder Data Collection

High-quality X-ray powder diffraction data were obtained for γ-$Zn_2P_2O_7$ with a Siemens D500 diffractometer with pure monochromated Cu$K\alpha_1$ radiation selected with an incident-beam curved-crystal germanium monochromator with asymmetric focusing (short focal distance 124 mm, long focal distance 216 mm). The alignment of the diffractometer was checked by means of the 00l reflections of fluorophlogopite mica (NIST SRM 675) (21). The zero error was estimated as less than 0.01° (2θ). The instrumental resolution function exhibits a shallow minimum of 0.065° (2θ) at about 40° (2θ) and has twice this value at 130° (2θ) (22). For comparison, the average value of FWHMs at 40° was 0.12° (2θ) for γ-$Zn_2P_2O_7$. The powder was mounted in a top-loaded sample holder. The stability of the material and the absence of significant preferred orientation of the crystallites were checked by preliminary data collections. The diffraction pattern was scanned over the angular range 10–150° (2θ), with a step length of 0.02° (2θ) and a counting time of 23 s $step^{-1}$ until 80° (2θ) and 46 s $step^{-1}$ to the end of the scan. The full pattern was then scaled to 23 s $step^{-1}$. After data collection, the stability of the X-ray source was checked by recording again the first lines. The extraction of peak positions for indexing was performed with the Socabim fitting program PROFILE, available in the PC software package DIFFRAC-AT supplied by Siemens. Phase identification was carried out with the program SEARCH/MATCH from Socabim, combined with the PDF1 data base (23). The program POWDER CELL was used for structure drawings (24).

THERMAL BEHAVIOR OF ZINC PHENYLPHOSPHONATE

Figure 1 shows the three-dimensional representation of the powder diffraction patterns obtained during the decomposition in air of $Zn(O_3PC_6H_5)\cdot H_2O$, in the temperature range 19–600°C. This plot reveals that the decomposition of the precursor proceeds through four stages. The TG curve is shown in Fig. 2. It exhibits only two successive weight losses in the same temperature range. These experimental results can be explained as follows.

(i) The precursor is stable until 75°C and then transforms into the anhydrous phase, $Zn(O_3PC_6H_5)$ (observed weight

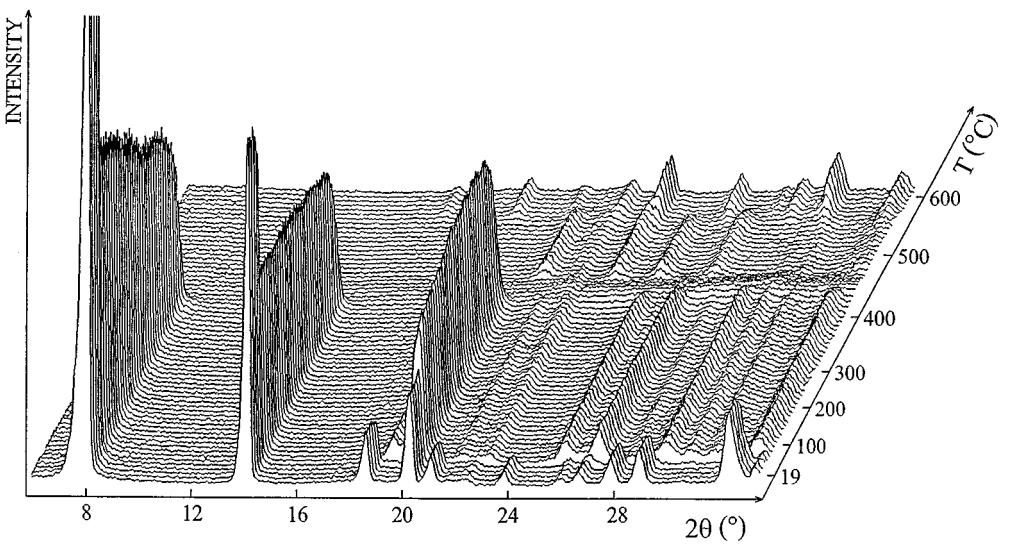

FIG. 1. TDXD plot for $Zn(O_3PC_6H_5)\cdot H_2O$.

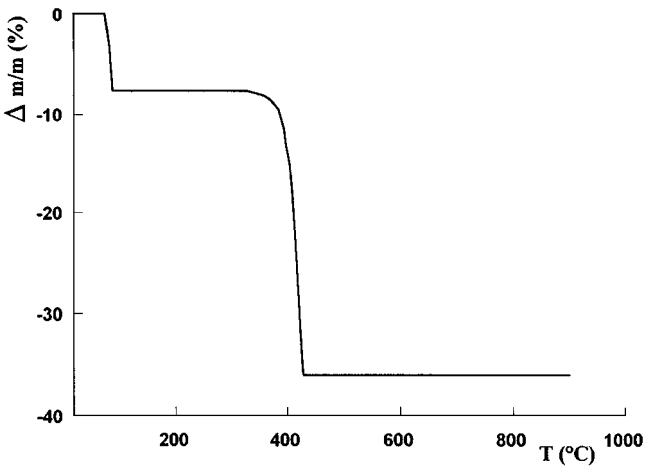

FIG. 2. TG curve for the decomposition in air of $Zn(O_3PC_6H_5)\cdot H_2O$.

loss, 7.6%; theoretical, 7.52%). These results agree with those reported by Frink *et al.* (6). As shown in the three-dimensional plot, the elimination of the coordinated water molecule occurs without a significant change in position of the strongest lines of the initial diffraction pattern, while their intensity decreases significantly and new lines appear. The powder diffraction pattern of the anhydrous phase has been indexed with the program DICVOL91 (25), leading to a monoclinic cell: $a = 14.492(5)$ Å, $b = 5.180(1)$ Å, $c = 5.289(1)$ Å, $\beta = 94.81(2)^\circ$. The powder data have been submitted to the ICDD (23) for possible inclusion in the Powder Diffraction File. This monoclinic unit cell characterized by satisfactory figures of merit [$M_{20} = 44$, $F_{25} = 61(0.0090,46)$] differs from the orthorhombic cell proposed by Frink *et al.* (6). It should be noted that the magnitude of the interlayer spacing $a \sin \beta$ ($= 14.441$ Å) is related to the spacing found in the hydrated phase (14.339 Å) (3), which suggests some structural relations between the two phases (6).

(ii) The anhydrous phase is remarkably stable until 330°C, from which the phase begins to decompose. The last plateau is observed on the TG curve from 430°C and remains constant until 900°C. The corresponding weight loss is 36.0%, which is in accordance with the formation of $Zn_2P_2O_7$ (theoretical weight loss: 36.38%). It is interesting to note that in the temperature range 430–600°C the TDXD plot displays several phases which must be explained by the existence of polymorphic varieties of zinc diphosphate.

(iii) Figure 1 shows that $Zn(O_3PC_6H_5)$ leads at 430°C to an amorphous phase with a global formula $Zn_2P_2O_7$ as shown from the TG curve (Fig. 2). Observations performed *ex situ* revealed that the powder obtained is black. Nevertheless, additional experiments carried out in air at 330°C, the onset temperature of the decomposition of $Zn(O_3PC_6H_5)$ in the TG experiment, showed that this amorphous polymorph was also formed in one month and that the material was thus white. No crystallization was observed with longer times at this temperature. This result suggests that the black color observed in the faster thermal treatment is likely due to residual carbon arising from the decomposition of the phenyl groups.

(iv) Amorphous $Zn_2P_2O_7$ crystallizes at 480°C to form the polymorph δ-$Zn_2P_2O_7$. The sample obtained is black when prepared with a fast thermal treatment, but it is white when it is prepared at 400°C in the oven over a few days. Powder diffraction data for the black and white samples of the phase δ showed that the materials were identical, though anisotropic diffraction line broadening was significant and was reduced from 0.45° (2θ) in the black sample to 0.30° (2θ) in the white sample. Nevertheless, no better crystallization was obtained with longer annealing times. The powder data for δ-$Zn_2P_2O_7$ are given in Table 1. Attempts to index these data were unsuccessful, due to the lack of resolution of the pattern. The density measured for this phase is $3.688\ g\,cm^{-3}$.

(v) The last stage observed on the TDXD plot (Fig. 1) is the formation at 550°C of a polymorph identified from the interrogation of the PDF1 database (PDF Nos. 39-711 and 43-488) (23). Despite low agreement, it was clear enough that the gray-phase obtained in the present study is γ-$Zn_2P_2O_7$. When cooled at room temperature the γ-phase remained stable. Similar behavior was observed with a white sample. The latter was formed in an oven after heating at 430°C white δ-$Zn_2P_2O_7$ for 1 week.

TABLE 1
X-ray Powder Data of δ-$Zn_2P_2O_7$

$2\theta_{EXP}$ (deg)	I/I_O	d_{EXP} (Å)
18.776	2	4.722
19.354	61	4.583
20.291	7	4.373
21.961	100	4.044
23.714	47	3.749
25.717	75	3.461
29.305	17	3.045
30.824	7	2.899
31.896	25	2.803
32.723	30	2.735
33.341	8	2.685
36.500	21	2.4597
37.709	7	2.3836
38.399	28	2.3423
39.128	13	2.3004
40.341	7	2.2340
41.315	2	2.1835
42.057	5	2.1467
42.865	5	2.1081
43.531	3	2.0774
44.158	6	2.0493

It is worth noting here the results reported recently by Petrova *et al.* (18) on the crystallization study of the glass $2ZnO \cdot P_2O_5$. Indeed, the phases observed during the thermal treatment of this glass seem similar to those described from amorphous $Zn_2P_2O_7$ formed from the decomposition of $Zn(O_3PC_6H_5)$. Consequently, the phases *x* and *y* observed by Petrova *et al.* (18) should be named δ- and γ-$Zn_2P_2O_7$, respectively. Additional reported data, e.g. density, agree well with the data reported here. It should also be mentioned that the transformation of γ-$Zn_2P_2O_7$ into β-$Zn_2P_2O_7$ reported at higher temperature (17), followed by the formation on cooling of α-$Zn_2P_2O_7$, was confirmed in the present study.

AB INITIO STRUCTURE DETERMINATION OF γ-$Zn_2P_2O_7$

Pattern Indexing

Indexing of the X-ray powder diffraction pattern was performed using the program DICVOL91 (25). The first 20 lines, with an absolute error of 0.03° (2θ) on peak positions, were indexed on the basis of an orthorhombic solution with the figures of merit $M_{20} = 29$ and $F_{20} = 54$ (0.0087, 43). The correctness of this solution was confirmed from a review of the powder data available, using the program NBS*AIDS83 (26). After this evaluation and refinement, the unit cell dimensions were $a = 4.9504(5)$ Å, $b = 13.335(2)$ Å, $c = 16.482(3)$ Å, and $V = 1088.1(2)$ Å^3 with $M_{20} = 35$ and $F_{30} = 76$ (0.0099, 40), according to the conditions for nonextinction. The powder data have been submitted to the ICDD (23) for possible inclusion in the Powder Diffraction File. The systematic absences were found to be consistent with the space groups $Pbc2_1$ and *Pbcm*. Moreover, the calculated density (3.719 g cm^{-3}), assuming a global formula $Zn_2P_2O_7$ and $Z = 8$, agrees well with both the observed value (3.716 g cm^{-3}) and that reported by Petrova *et al.* (18) (3.72 ± 0.01 g cm^{-3}) for a phase referenced as *y*. It is interesting to note that the density values, 4.2 g cm^{-3} (15) and 4.247 g cm^{-3} (16), calculated for the α and β varieties are somewhat different. Therefore, the structure of γ-$Zn_2P_2O_7$ appears as less compact than that of the two other polymorphs. This is confirmed by calculating the chemical-formula-unit equivalent volume V_{eq} ($= V_{cell}/Z$) for each variety, i.e., 120.6 and 119.1 Å^3 for phases α and β and 136.0 Å^3 for γ-$Zn_2P_2O_7$.

As indicated above, two powder diffraction patterns for $Zn_2P_2O_7$ [PDF files No. 39-711 and No. 43-488] have been reported without indexing, in addition to the data for the phase *y* (18). They have been analyzed from the solution reported in the present study. The corresponding figures of merit [$M_{20} = 7$ and $F_{21} = 9$ (0.0231, 99) for file No. 39-711; $M_{19} = 5$ and $F_{29} = 10$ (0.0439, 67) for file No. 43-488; $M_{18} = 7$ and $F_{28} = 6$ (0.0264, 168) for phase *y* (18)] reflect the poor quality of these powder data.

The orthorhombic unit cell of γ-$Zn_2P_2O_7$ was used to interrogate the NIST-CDF database (27). No isostructural related material was detected. Nevertheless, it is worth noting the crystallographic relationship between the γ form and the monoclinic variety β [PDF File No. 34-1275 and Ref. (16)]. This is apparent from the application of the transformation matrix [0, $\frac{1}{2}$, 0/0, 0, $\frac{1}{2}$/1, 0, 0] to the orthorhombic cell of γ-$Zn_2P_2O_7$, from which results a new parameter setting: $a' = 6.668$ Å, $b' = 8.242$ Å, $c' = 4.9504$ Å, and $V' = 272.0$ Å^3. This cell presents some parametric analogies with the cell of β-$Zn_2P_2O_7$ (16), i.e., $a = 6.61(1)$ Å, $b = 8.29(1)$ Å, $c = 4.51(1)$ Å, $\beta = 105.4(2)°$, and $V = 238.3$ Å^3 ($Z = 2$). This feature may reflect structural analogies between the structure of the γ phase and that of the β phase, in which the γ phase transforms upon heating. To shed light on these apparent crystallographic relationships, the structure of γ-$Zn_2P_2O_7$ is obviously needed. Since no single crystals were obtained for this variety, a powder sample was prepared from the thermal decomposition in air of $Zn(O_3PC_6H_5) \cdot H_2O$ at 600°C. X-ray powder data were collected at room temperature. Two spurious diffraction lines with low intensity, located at 29.42 and 29.68° (2θ), were detected in the pattern. They were attributed to α-$Zn_2P_2O_7$ from the interrogation of the PDF1 data base (23). These lines are the strongest with the pattern of the α phase and correspond to 3% of the strongest line observed for the γ phase. The structure of γ-$Zn_2P_2O_7$ was solved from these powder data assuming the centrosymmetric space group.

Structure Determination

Integrated intensities were extracted with the program EXTRA (28), based on the iterative decomposition algorithm introduced first by Le Bail *et al.* (29). In the angular range 10–80° (2θ), 347 structure factor amplitudes were obtained, including 41.6% of symmetry-independent reflections. They were input in the direct-methods program SIRPOW.92 (30). All 14 atoms were found from the first 15 peaks generated from the *E* map with the highest figure of merit. Among the 14 independent atoms two phosphorus and 4 oxygen atoms lie on special positions (see Table 3). The refinement of the atomic coordinates of Zn, P, and O led to a residual value $R = 11.9\%$. At this stage, the molecular geometry displayed by the program SIRPOW.92 was in agreement with the presence of diphosphate groups and two 5-fold coordinated zinc atoms. A least-squares Rietveld refinement using the program FULLPROF (31) was carried out in the angular range 10–150° (2θ), containing 1166 reflections. A pseudo-Voigt function was selected to describe individual line profiles, with a possible variation of the mixing factor η. The refinement involved the following parameters: 49 atomic parameters (including 14 isotropic atomic displacement parameters), 1 scale factor, 1 zero-point, 3 cell parameters, 3 half-widths and 1 line

TABLE 2
Details of the Rietveld Refinement for γ-$Zn_2P_2O_7$

Space group	*Pbcm*
Z	8
Wavelength (Å)	1.5406
2θ range (deg)	10–150
Step scan increment (2θ, deg)	0.02
No. of atoms	14
No. of reflections	1166
No. of structural parameters	50
No. of profile parameters	15
R_F	0.041
R_B	0.061
R_p	0.116
R_{wp}	0.150

asymmetry parameter, 2 variables for the angular variation of η, and 5 coefficients used to describe the functional dependence of the background. The refinement converged to satisfactory residual factors $R_F = 0.041$ and $R_{wp} = 0.150$. No improvement was observed in refining the preferred orientation parameter. The details of the Rietveld refinement are reported in Table 2. Figure 3 shows the final Rietveld plot. The residuals observed on the difference plot may be partly explained by the presence of about 3% of the impurity phase discussed above and, also, to a small anisotropic line-broadening effect. It is interesting to note that a very similar difference curve was observed in the pattern matching stage for extracting integrated intensities, in which no structure model is involved. It can then be concluded that the discrepancies arise more from imperfect analytical modeling of a few lines with different shape factors than from small structural imperfections. The final atomic positions and atomic displacement parameters are given in Table 3. Table 4 displays bond distances and angles in the structure.

TABLE 3
Fractional Atomic Coordinates and Isotropic Atomic Displacement Parameters for γ-$Zn_2P_2O_7$

Atom	Site	x	y	z	B_{iso} (Å^2)
Zn1	8*e*	0.0948(4)	0.0453(2)	0.5867(2)	1.25(5)
Zn2	8*e*	0.3202(4)	0.2575(2)	0.6564(1)	1.13(5)
P1	8*e*	0.5777(9)	0.1435(3)	0.4974(3)	0.89(9)
P2	4*d*	0.825(1)	0.1502(5)	0.75	1.3(1)
P3	4*d*	− 0.033(1)	− 0.0578(5)	0.75	1.0(1)
O1	8*e*	0.118(2)	− 0.0501(7)	0.6745(5)	0.8(2)
O2	8*e*	0.408(2)	0.1415(6)	0.5710(6)	0.5(2)
O3	8*e*	0.810(2)	0.0637(7)	0.5007(6)	1.2(2)
O4	8*e*	0.406(2)	0.3635(6)	0.5793(6)	0.3(2)
O5	4*d*	0.558(3)	0.209(1)	0.75	0.6(3)
O6	4*c*	0.734(2)	0.25	0.5	0.8(3)
O7	8*e*	− 0.023(2)	0.1692(7)	0.6725(6)	1.4(3)
O8	4*d*	0.744(2)	0.035(1)	0.75	0.6(3)
O9	4*d*	0.215(3)	0.349(1)	0.75	2.1(4)

DESCRIPTION OF THE STRUCTURE

A projection of the three-dimensional structure of γ-$Zn_2P_2O_7$ onto the (100) plane (Fig. 4) shows that the structure can be described from a framework with lower dimensionality. It is built from edge-sharing ZnO_5 polyhedra forming corrugated chains running along [001]. The P_2O_7 groups ensure both the cohesion within a chain and the propagation of the structure by connecting the chains together along the two other cell directions. The projection of the corrugated chains along [001] displayed in Fig. 5 shows that two adjacent chains in the direction of *b* axis make an angle enforced by the P–O_b–P angle of the diphosphate groups. The zinc atoms adopt a 5-fold coordination in the form of slightly distorted trigonal bipyramids (Fig. 6). They are linked within a chain according to the sequence [… Zn1–O_2–Zn1–O_2–Zn2–O_2–Zn2 …], which is characterized by an alternation of two distinct pairs of zinc atoms as illustrated in Fig. 4. The two $Zn1O_5$ and $Zn2O_5$ polyhedra have the O2–O7 edge in common, whereas the $O3^I$–$O3^{II}$ and O5–O9 edges bridge two $Zn1O_5$ and two $Zn2O_5$ units, respectively. The Zn–Zn distances within a chain fall into two groups: 3.084 Å, involving only Zn2 atoms running parallel to the *c* axis, and 3.242 Å between two Zn1 atoms, which is close to the Zn1–Zn2 distance, i.e., 3.252 Å. The Zn1–O distances vary from 1.930(9) to 2.25(1) Å [mean value 2.06(1) Å] while the Zn2–O distances lie between 1.949(9) and 2.136(9) Å [mean value 2.049(9) Å]. Moreover, it is noticeable that the lowest distances in the two polyhedra are between zinc atoms and the unshared oxygen atom, i.e., Zn1–O1 and Zn2–O4. In order to confirm the 5-fold coordination for zinc atoms, calculations of bond distances in various polyhedra were performed with the program VALENCE (32). The coordination numbers 4, 5, and 6 were chosen for the zinc element. A theoretical bond distance of 2.04 Å for a 5-fold coordination was obtained, in agreement with the mean values calculated above for the two polyhedra. Furthermore, calculations for 4- and 6-fold coordinations led to bond distances of 1.96 and 2.11 Å, respectively, making unlikely these coordination numbers. As already mentioned, zinc atoms are in somewhat distorted trigonal bipyramids (Fig. 6). The axial $O3^{II}$–Zn1–O7 and O2–Zn2–O9 angles are 175(1) and 170(6)°, not too far from the ideal value of 180°. The deviation of Zn1 and Zn2 from the plane of the triangles $O1O2O3^I$ and O4O5O7 are 0.029 and 0.026 Å, respectively. According to the distances between zinc atoms and these oxygen atoms, this result remarkably points out the unusual geometry adopted by the two zinc atoms. The two independent $P_2O_7^{4-}$ anions exhibit nonlinear P–O_b–P bonds, both with rather low angles, i.e., 122.9(8)° for P1–O6–P1 and 124(2)° for P2–O8–P3, and

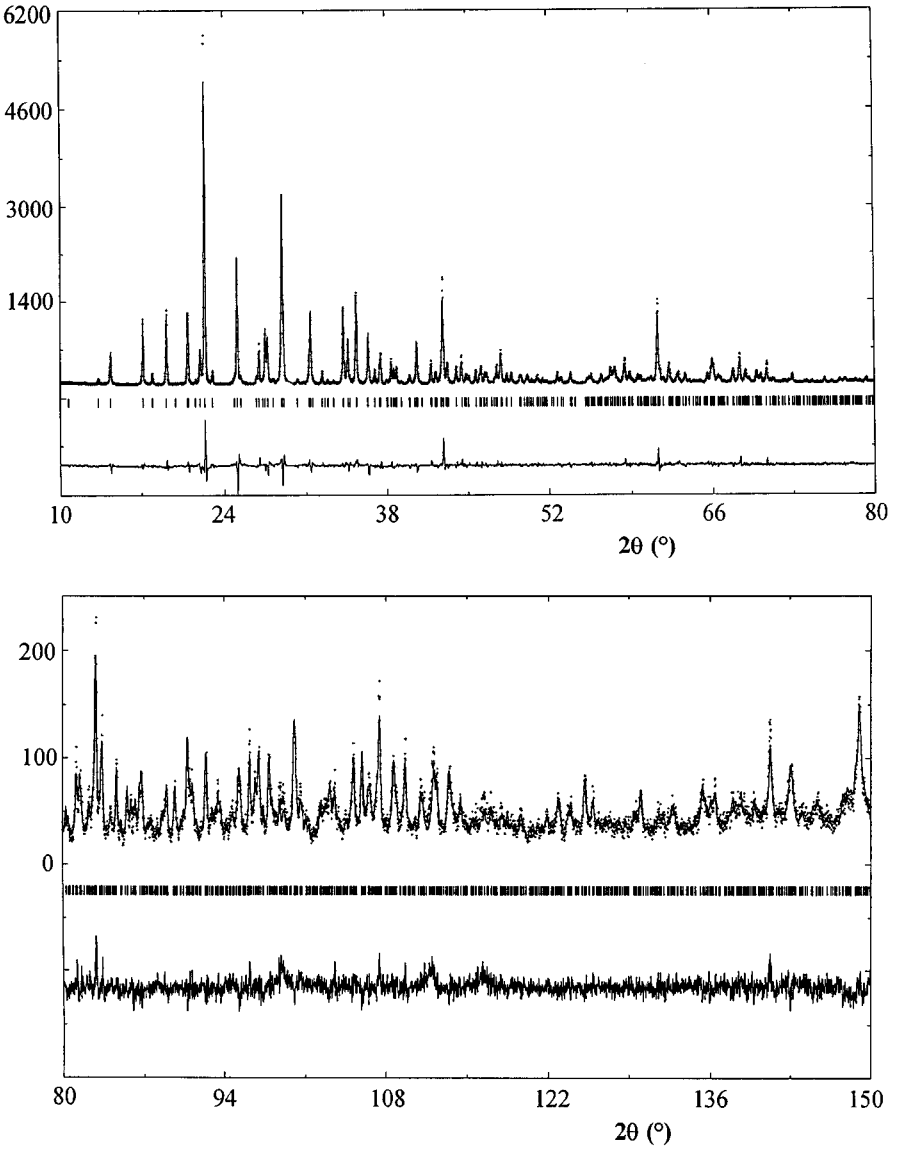

FIG. 3. Final Rietveled plot for γ-$Zn_2P_2O_7$. The upper trace shows the observed data as dots, while the calculated pattern is shown by the solid line. The lower trace is a plot of the difference: observed minus calulated. Note that the intensity scale is different for the high-angle region.

show an eclipsed conformation. The PO_4 tetrahedra present one long P–O distance with the bridging oxygen atom (average 1.619 Å) and three shorter distances with the terminal oxygen atoms (average 1.513 Å), in accordance with the discussion developed by Baur (33) regarding to the predictive relationships for the phosphate groups.

DISCUSSION

Zinc atoms with coordination number 5 have also been observed in the structure of α-$Zn_2P_2O_7$ (15). However while all zinc atoms in γ-$Zn_2P_2O_7$ are 5-fold coordinated, their coordination is both 5 and 6 in α-$Zn_2P_2O_7$ and only 6 in the high-temperature form β-$Zn_2P_2O_7$. It is, to our knowledge, the first time in the family of phosphates that all Zn atoms in the structure are 5-fold coordinated. Moreover, mixed coordination numbers are also found in pure γ-$Zn_3(PO_4)_2$ (34). Nord and Kierkegaard (35) showed that two-thirds of the Zn atoms were 5-fold coordinated, in the shape of distorted trigonal bipyramids (36). In γ-$Zn_2P_2O_7$, the two highest bond lengths are related to the axial distances Zn1–O7 and Zn2–O2. The same feature, but more noticeable, was also pointed out in the ZnO_5 polyhedra of γ-$Zn_3(PO_4)_2$, in which the highest value is 2.40 Å [see Table 3 of Ref. (37)]. This observation was later extended to the farringtonite phases, $(Zn_{1-x}Mg_x)_3(PO_4)_2$, in which the axial

TABLE 4
Selected Bond Distances (Å) and Angles (°) with Their Standard Deviations for γ-$Zn_2P_2O_7$

		Within the ZnO_5 polyhedra	
Zn1–O1	1.930(9)	Zn2–O2	2.136(9)
Zn1–O2	2.029(9)	Zn2–O4	1.949(9)
Zn1–O3^{I}	2.01(1)	Zn2–O5	2.048(9)
Zn1–O3^{II}	2.10(1)	Zn2–O7	2.08(1)
Zn1–O7	2.25(1)	Zn2–O9	2.03(1)
		Within the P_2O_7 groups	
		O2–P1–O3	112(1)
P1–O2	1.48(1)	O2–P1–O4^{III}	111(1)
P1–O3	1.57(1)	O2–P1–O6	105.4(9)
P1–O4^{III}	1.53(1)	O3–P1–O4^{III}	113(1)
P1–O6	1.617(7)	O3–P1–O6	104.1(8)
		O4^{III}–P1–O6	110(1)
	P1–O6–P1^{III}	122.9(8)	
		O5–P2–O7^{IV}	110(1)
P2–O5	1.53(2)	O5–P2–O7^{V}	110(1)
P2–O7^{IV}	1.50(1)	O5–P2–O8	106(2)
P2–O7^{V}	1.50(1)	O7^{IV}–P2–O7^{V}	116(1)
P2–O8	1.59(2)	O7^{IV}–P2–O8	107(1)
		O7^{V}–P2–O8	107(1)
		O1–P3–O1^{VI}	117(1)
P3–O1	1.46(1)	O1–P3–O8^{I}	107(1)
P3–O1^{VI}	1.46(1)	O1^{VI}–P3–O8^{I}	107(1)
P3–O8^{I}	1.65(2)	O1–P3–O9^{VII}	111(2)
P3–O9^{VII}	1.54(2)	O1^{VI}–P3–O9^{VII}	111(2)
		O8^{I}–P3–O9^{VII}	103(2)
	P2–O8–P3^{IV}	124(2)	

Note. Symmetry code: I, $x-1, y, z$; II, $1-x, -y, 1-z$; III, $x, 0.5-y, 1-z$; IV, $1+x, y, z$; V, $1+x, y, 1.5-z$; VI, $x, y, 1.5-z$; VII, $-x, y-0.5, z$.

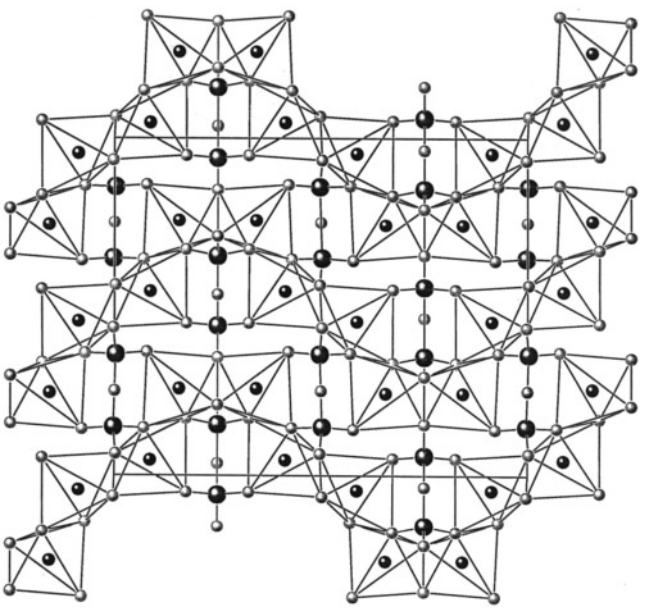

FIG. 4. View of the unit cell of γ-$Zn_2P_2O_7$ along the *a* axis, with *b* vertical and *c* horizontal. Large black circles, P atoms; small black circles, Zn atoms; grey circles, O atoms.

distances range from 2.32 Å for $x = 0.27$ to 2.19 Å for $x = 0.80$ (38). Moreover, the average Zn–O distances [2.06(1) and 2.049(9) Å] in γ-$Zn_2P_2O_7$ can be compared with those observed in α-$Zn_2P_2O_7$ (2.038 and 2.027 Å for the two 5-coordinated zinc atoms) (15), in γ-$Zn_3(PO_4)_2$ (2.05 Å) (37) and in the farringtonite phases (2.05 Å until $x = 0.5$ and 2.03 Å for $x > 0.5$) (38).

In the structure of γ-$Zn_2P_2O_7$, the bond lengths and the angles P–O_b–P agree well with the dimensions reported for various diphosphate anions (see Refs. (14) and (39)). It is interesting to mention here the plot P–O_b–P (deg) *versus* P–O_b (Å) reported by Mandel (Fig. 2 in Ref. (39)) which

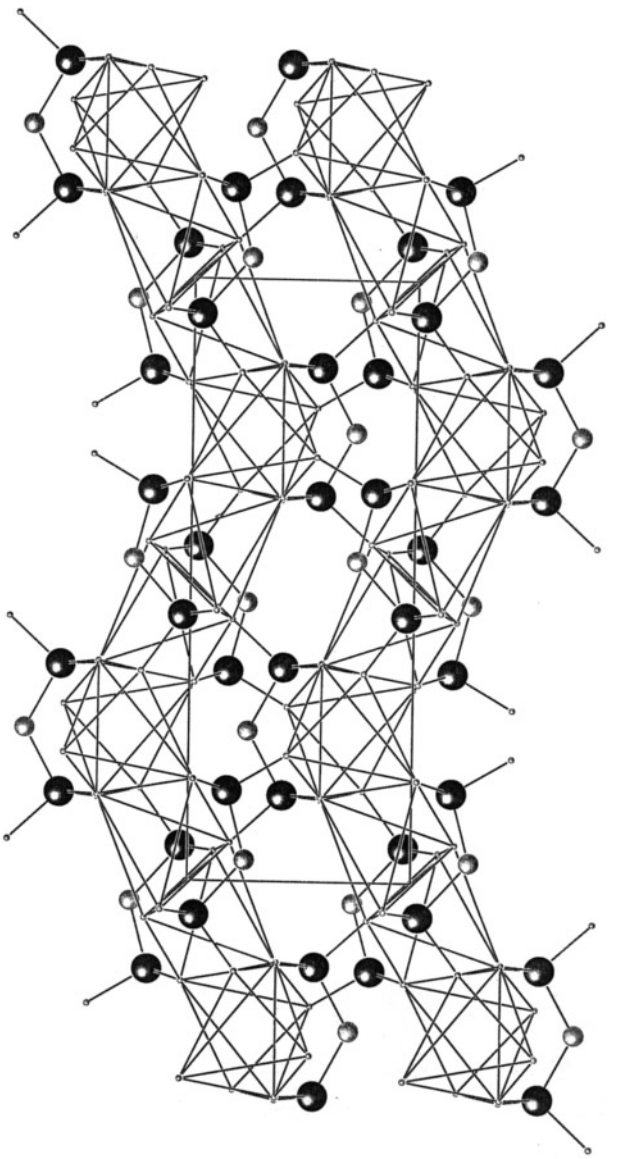

FIG. 5. Projection of the structure of γ-$Zn_2P_2O_7$ along the *c* axis (*b* vertical and *a* horizontal). For clarity Zn atoms and O atoms are omitted, except bridging diphosphate O atoms.

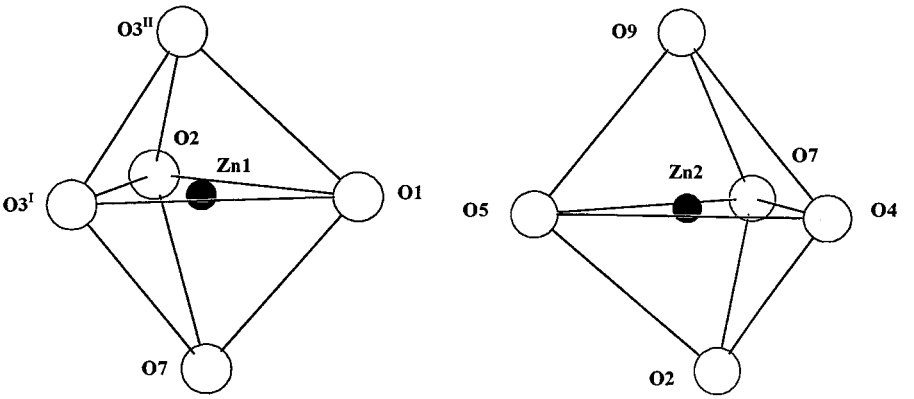

FIG. 6. View of the environment of Zn atoms.

illustrates the strong relationship between the phosphorus-bridging oxygen bond length (1.63–1.54 Å) and the bridging angle (123–180°), covering both wide ranges. Indeed, the longest P–O_b distances ($\approx$ 1.63 Å) correlates well with the smallest P–O_b–P angles ($\approx$ 123°) and, inversely, the shortest distances ($\approx$ 1.54 Å) with the largest angles (formal 180°). The angle values reported here for γ-$Zn_2P_2O_7$ are located satisfactorily at the lower angle limit in the plot. A similar feature is observed in the phases α-$Na_2CuP_2O_7$ and β-$Na_2CuP_2O_7$, in which the P–O–P angles are remarkably low, i.e., 118.7(2) and 120.2(1)°, and are accompanied by long P–O_b distances, 1.633(2) and 1.613(1) Å, respectively (40).

The two P_2O_7 groups in γ-$Zn_2P_2O_7$ exhibit an eclipsed conformation, as it is observed in the compounds $A_2P_2O_7$ where A is a large cation with a ionic radius greater than 0.97 Å, e.g., Ca, Sr, Ba, Pb. The last are related to the dichromate-type compounds (41). At the opposite, $A_2P_2O_7$ compounds with ionic radii of A less than 0.97 Å are related to the thortveitite-type structure. This type includes the two zinc diphosphate polymorphs α and β, and some other 3*d* transition metal diphosphates, in which the P_2O_7 groups display a staggered conformation. With regard to the conformation and the distortions within P_2O_7 groups in γ-$Zn_2P_2O_7$, it is clear that the structure is far from the thortveitite type. Surprisingly, γ-$Zn_2P_2O_7$ can be included in the dichromate-type compounds, even though the ionic radius of Zn^{2+} does not correspond to those predicated by the type of the structure. This observation is likely to be related to the fact that the chemical-formula-unit equivalent volume V_{eq}^{γ} for γ-$Zn_2P_2O_7$ is notably different from the two close volumes, V_{eq}^{α} and V_{eq}^{β}, calculated for α-$Zn_2P_2O_7$ and β-$Zn_2P_2O_7$. In the same way, from the density of δ-$Zn_2P_2O_7$ (3.688 g cm^{-3}), close to the density of γ-$Zn_2P_2O_7$ (3.716 g cm^{-3}), it can be suggested that the δ phase would crystallize with the dichromate-type structure. Unfortunately, the quality of the powder data is not good enough to undertake a structure study.

To conclude, temperature-dependent X-ray powder diffraction has revealed the existence of $Zn_2P_2O_7$ polymorphs, which could not be identified by TG measurements, illustrating again the power of this technique. The structure of γ-$Zn_2P_2O_7$ has been completely solved *ab initio* from powder diffraction data collected with a conventional X-ray source. The polymorph γ crystallizes with a new structure type, by comparison with the two other polymorphs α and β.

ACKNOWLEDGMENTS

The authors are grateful to Pr. J. P. Auffrédic for helpful discussions on TG measurements and to Mr. G. Marsolier for his technical assistance.

REFERENCES

1. D. Cunningham, P. J. D. Hennelly, and T. Deeney, *Inorg. Chim. Acta* **37,** 95 (1979).
2. G. Cao, H. Lee, V. M. Lynch, and T. E. Mallouk, *Inorg. Chem.* **27,** 2781 (1988).
3. K. J. Martin, P. J. Squattrito, and A. Clearfield, *Inorg. Chim. Acta* **155,** 7 (1989).
4. Y. Ortiz-Avila, P. R. Rudolf, and A. Clearfield, *Inorg. Chem.* **28,** 2137 (1989).
5. G. Cao and T. E. Mallouk, *Inorg. Chem.* **30,** 1434 (1991).
6. K. J. Frink, R.-C. Wang, J. L. Colón, and A. Clearfield, *Inorg. Chem.* **30,** 1438 (1991).
7. J. Le Bideau, A. Jouanneaux, C. Payen, and B. Bujoli, *J. Mater. Chem.* **4**(8), 1319 (1994).
8. S. Drumel, P. Janvier, P. Barboux, M. Bujoli-Dœuff, and B. Bujoli, *Inorg. Chem.* **34,** 148 (1995).
9. D. M. Poojary and A. Clearfield, *J. Am. Chem. Soc.* **117,** 11278 (1995).
10. D. M. Poojary, B. Zhang, P. Bellinghausen, and A. Clearfield, *Inorg. Chem.* **35,** 5254 (1996).
11. D. Massiot, S. Drumel, P. Janvier, M. Bujoli-Dœuff, and B. Bujoli, *Chem. Mater.* **9,** 6 (1997).
12. A. Cabeza, M. A. G. Aranda, F. M. Cantero, D. Lozano, M. Martinez-Lara, and S. Bruque, *J. Solid State Chem.* **121,** 181 (1996).
13. C. G. Lugmair, T. D. Tilley, and A. L. Rheingold, *Chem. Mater.* **9,** 339 (1997).
14. A. Durif, "Crystal Chemistry of Condensed Phosphates." Plenum Press, New York, 1995.

15. B. E. Robertson and C. Calvo, *J. Solid State Chem.* **1,** 120 (1970).
16. C. Calvo, *Can. J. Chem.* **43,** 1147 (1965).
17. A. Kishioka, K. Itatani, and M. Kinoshita, *J. Ceram. Assoc. Jpn.* **93**(10), 606 (1985).
18. M. A. Petrova, V. I. Shitova, G. A. Mikirticheva, V. F. Popova, and A. E. Malshikov, *J. Solid State Chem.* **119,** 219 (1995).
19. P. Bénard, J. P. Auffrédic, and D. Louër, *Mater. Sci. Forum* **228–231,** 325 (1996).
20. J. Plévert, J. P. Auffrédic, M. Louër, and D. Louër, *J. Mater. Sci.* **24,** 1913 (1989).
21. D. Louër, *in* "Accuracy in Powder Diffraction II" (E. Prince and J. K. Stalick, Eds.), pp. 92–104. NIST Spec. Publication No. 846, NIST, Gaithershurg, MD, 1992.
22. D. Louër and J. I. Langford, *J. Appl. Crystallogr.* **21,** 430 (1988).
23. International Centre for Diffraction Data, PDF Database, Newtown Square, PA.
24. W. Kraus and G. Nolze, *J. Appl. Crystallogr.* **29,** 301 (1996).
25. A. Boultif and D. Louër, *J. Appl. Crystallogr.* **24,** 987 (1991).
26. A. D. Mighell, C. R. Hubbard, and J. K. Stalick, "NBS*AIDS80: A FORTRAN Program for Crystallographic Data Evaluation." US Technical Note 1141, National Bureau of Standards, Washington, DC, 1981. [NBS*AIDS83 is an expanded version of NBS*AIDS80].
27. International Centre for Diffraction Data, NIST CDF Database, Newtown Square, PA.
28. A. Altomare, M. C. Burla, G. Cascarano, C. Giacovazzo, A. Guagliardi, A. G. G. Moliterni, and G. Polidori, *J. Appl. Crystallogr.* **28,** 842 (1995).
29. A. Le Bail, H. Duroy, and J. L. Fourquet, *Mater. Res. Bull.* **23,** 447 (1988).
30. A. Altomare, G. Cascarano, C. Giacovazzo, A. Guagliardi, A. G. G. Moliterni, M. C. Burla, and G. Polidori, *J. Appl. Cryst.* **28,** 738 (1995).
31. J. Rodriguez-Carvajal, *in* "Collected Abstracts of Powder Diffraction Meeting, Toulouse, France, 1990," p. 127.
32. I. D. Brown, *J. Appl. Crystallogr.* **29,** 479 (1996).
33. W. H. Baur, *Acta Crystallogr., Sect. B* **30,** 1195 (1974).
34. C. Calvo, *J. Phys. Chem. Solids* **24,** 141 (1963).
35. A.G. Nord and P. Kierkegaard, *Chem. Scr.* **15,** 27 (1980).
36. A.G. Nord and T. Stefanidis, *Mater. Res. Bull.* **16,** 1121 (1981).
37. A.G. Nord, *Mater. Res. Bull.* **12,** 563 (1977).
38. P. Bénard, A. G. Nord, P.-E. Werner, and M. Westdahl, *J. Solid State Chem.* **99,** 290 (1992).
39. N. S. Mandel, *Acta Crystallogr., Sect. B* **31,** 1730 (1975).
40. F. Erragh, A. Boukhari, F. Abraham, and B. Elouadi, *J. Solid State Chem.* **120,** 23 (1995).
41. A. A. El Belghitti, A. Elmarzouki, A. Boukhari, and E. M. Holt, *Acta Crystallogr., Sect. C* **51,** 1478 (1995).